UMERC+OREC
2025 Conference

12-14 August | Corvallis, OR USA

Deep Learning Based Ocean Current Feature Detection for Prediction

Louis DeVito[a], Sasha Fung[b], James VanZwieten[a], Yufei Tang[b], Laurent Chérubin[a]

[a]Florida Atlantic University, Department of Ocean and Mechanical Engineering
[b]Florida Atlantic University, Department of Electrical Engineering and Computer Science

Abstract

Ocean current prediction remains valuable for renewable energy exploitation and environmental management. Building on previous studies that quantified ocean current flows through direct measurements and numerical models, the present research advances the field by focusing on refined feature extraction techniques to forecast extreme current events. Prior work has examined detection tools for ocean eddies and current boundaries, as well as extreme event mapping at proposed energy production sites like the Florida Current (FC). Such developments have established a foundation for enhanced analysis of ocean dynamics and the identification of persistent flow structures.

This paper entails the implementation of a deep learning data fusion tool combining multiple sources of oceanographic data to identify ocean features in the FC. Promising results have been obtained. Future work envisions integrating the developed data fusion tool into an advanced deep learning ocean current prediction model pertaining to the FC. This integration will extend the application of convolutional neural networks (CNNs) from feature extraction to full-scale predictive analytics, harnessing the power of fused multi-sensor data to model the intricate, nonlinear interactions that govern ocean current dynamics.

Keywords: Ocean current reconstruction; Ocean current feature detection; Edge detection; U-net; High-frequency radar

1. Introduction

Detecting oceanographic features that impact ocean current flow speeds as well as predicting their presence is crucial for accurately understanding the impacts on harvesting ocean current energy. Copious sources of data collecting measurements on ocean characteristics assist in identifying these features, such as satellite-measured sea surface temperature (SST) and sea surface chlorophyll-a (SSCa). Additionally, data from high-frequency (HF) radar technology quantifies surface current magnitudes and directions, effectively illustrating oceanic flow patterns at a particular timestep. Combining disparate data, such as satellite and HF radar observations, is important for garnering a deeper comprehension as to how these features interact within ocean current systems. Prior work has examined detection tools for ocean eddies and current boundaries, as well as extreme event mapping at proposed energy production sites like the Florida Current (FC). For instance, [1] descriptively portrays a comparative analysis amongst disparate forms of oceanographic satellite data, such as surface temperature, height, chlorophyll-a, and salinity, for discerning oceanic features. Additionally, an evaluation of sea surface temperature perturbations with concurrent edge detection during times of aberrant flow speeds measured by in situ instrumentation is delineated in [2]. Furthermore, deep learning has been instrumental in predicting such features from inputting the aforementioned forms of data. For instance, researchers in [3] compared prediction models using HF radar measurements corresponding to the Gulf of Thailand and concluded that a spatiotemporal convolutional neural network (CNN) along with a gated recurrent unit (GRU) provided results with minimal mean squared errors. An analysis in [4] demonstrated the success of predicting ocean currents in the Gulf of Thailand using HF radar measurements by introducing a temporal kNN model. Another study presented in [5] utilized a modified U-net model where the model's segmentation layer was replaced with a regression layer to provide both hindcasts and forecasts of ocean currents. A U-net model had also been implemented in [6] by inputting a multi-channel image consisting of SST, sea surface altimetry, and zonal and meridional flow speed observations to predict surface currents in the Mediterranean Sea. Research conducted in [7], [8], and [9] have contributed to this area of study in several ways, such as characterizing ocean currents from acoustic Doppler current profilers using a Long Short-Term Memory (LSTM) recurrent neural network, utilizing linear regression models and artificial neural networks to delineate surface flows by inputting variables like SST and wind stress, and a deep learning model with a weight loss function applied to SSC data with reductions in root mean square errors by over 10% and mean absolute errors over 13%.

The proposed methodology in this paper integrates high-resolution SST, SSCa, and HF radar to construct a newly developed data fusion tool. This data fusion tool consists of a CNN model, which is employed to automate the detection and extraction of these features. This framework delineates the identification and prediction of ocean current features within the FC system using measurements from various data sources between the years of 2014 and 2016. Specifically, data from 2014 and 2015 entail the model's training set, while data from 2016 encompass the model's testing set. The description of this data fusion model will be outlined as follows: Section 2 outlines the processing steps and results for the reconstruction U-net model, Section 3 does the same for the edge detection using attention U-net model, and Section 4 summarizes the results and details future works.

2. High-Frequency Radar Data Reconstruction via U-net

2.1. Pre-processing of Raw Data

HF radar datasets were obtained from two sites observing Florida Current flows near 26°N latitude: Dania Beach (STF) and Virginia Key (VIR). The data are organized by time step, with measurements recorded hourly in Coordinated Universal Time (UTC). Each radar measures the radial velocity of the flow, which is then converted into surface current velocities (zonal and meridional) using a weighted least-squares (WLS) approach. The datasets also include ancillary variables such as bearing angles, radial-velocity variance, radial-velocity accuracy, and measurement range. Before computing the surface currents, raw radial-velocity values are interpolated onto a regular latitude–longitude grid at 0.0275° resolution.

Certain quality control measures are utilized, such as in [10] and [11], are applied to ensure the reliability of surface flow speed calculations from the raw radial velocity data. The following quality-control filters are applied to remove unreliable measurements:

- **Bragg Scattering Threshold**: Radial velocity quantities exceeding a velocity related to Bragg scattering, which is 4.4125 m/s in this application.
- **Range Threshold**: Measurements surpassing 80 km from the HF radar instruments since the HF radar signal attenuates with distance.
- **Accuracy Threshold**: Radial velocity values with errors surpassing 8 cm/s.
- **Azimuthal Span**: Data from both radars that do not overlap in the specified bearing angle range (50°-148°) so that each data point is associated with two radial velocities, with one being measured from each radar.
- **Radial Velocity Magnitude**: Magnitudes of radial velocities greater than 3 m/s, since radial velocity magnitudes do not exceed this value along the waters off the southeastern United States.
- **GDOP Threshold**: Measurements containing a geometric dilution of precision (GDOP) above 2.5.

Although HF radar provides valuable snapshots of local flow, data gaps can occur due to maintenance, weather, interference, or antenna issues. Therefore, accurate reconstruction during periods of limited coverage is essential for downstream feature detection and forecasting. We employ a U-Net convolutional neural network to perform spatiotemporal inpainting of the zonal (east–west) and meridional (north–south) velocity components.

2.2. Dual-Radar Surface Current Reconstruction

To accurately reconstruct the surface current profiles, a coverage area is designated to illustrate the localized flow magnitudes and directions within the FC. This coverage area for measurements obtained each hour encompasses a latitudinal range between 25.51°N and 26.26°N as well as a longitudinal range between 79.48°W and 80°W. Hourly measurements associated with data completeness under 30% are removed and utilized for a separate test set.

As previously stated, the two radial components from each station were merged into orthogonal zonal (u) and meridional (v) velocities using a weighted least squares (WLS) solution. The WLS method was designated for its preservation of flow velocity gradients by accounting for the variance of radial velocity measurements at both HF radar locations. By considering the weights, which are the reciprocal of the variance values, any measurement noise from unreliable data present after the steps involving the quality control measures will be mitigated. The radial velocities (r) for valid data points are related to the zonal and meridional surface current components by considering the bearing angles (θ) associated with the HF radar measurements. For each data point:

$$\begin{bmatrix} r_1 \\ r_2 \end{bmatrix} = \begin{bmatrix} -\sin\theta_1 & -\cos\theta_1 \\ -\sin\theta_2 & -\cos\theta_2 \end{bmatrix} \begin{bmatrix} u \\ v \end{bmatrix}$$

The surface current vectors encompassing both the zonal and meridional components of the FC flows are calculated as follows:

$$\vec{a} = (A^T W A)^{-1} A^T W \vec{r}$$

where in this equation, a represents the surface-current vectors, A is the design matrix, W contains measurement weights, and r is the radial-velocity vector. The reconstructed fields were saved as hourly datasets for model training and evaluation. Approximately 15% of the time steps were omitted due to inadequate radar coverage or missing data.

2.3. U-net Reconstruction Results

The network follows a classic U-shaped encoder–decoder: the encoder repeatedly applies two 3×3 convolutions (with ReLU) followed by 2×2 max-pooling to down-sample and double the feature channels (32→64→128), the bottleneck consists of two 128-filter convolutions, and the decoder mirrors this with transposed convolutions to up-sample, concatenated skip-connections from the encoder, and two 3×3 conv layers per stage before a final 1×1 conv that linearly maps to the two output channels (u and v).

The model is evaluated on two sets: a standard test set consisting of hourly data of partial fields with at least 30% data coverage, and a “sparse test set" comprising spatially limited but partially valid fields excluded from training. Table 1 summarizes the reconstruction accuracy in terms of Mean Absolute Error (MAE), Mean Squared Error (MSE), Root Mean Squared Error (RMSE), and Coefficient of Determination (R^2).

Figure 1 illustrates representative reconstruction results for both u and v components. The model successfully recovers coherent flow patterns and velocity gradients, particularly in regions with strong advection. While performance degrades on the small test set due to limited spatial support, the method remains robust in reconstructing plausible fields.

Table 1: Reconstruction performance metrics for U and V components on the standard test set

Component	MAE	MSE	RMSE	R^2
U	0.0351	0.0025	0.0496	0.9703
V	0.0276	0.0018	0.0419	0.9809

In evaluating the deep-learning reconstruction, the error magnitudes remain on the order of only a few hundredths of a meter per second for both components, demonstrating sub-decimetric accuracy in the recovered fields. The coefficients of determination, R^2_U and R^2_V, both exceed 0.97, indicating that the network explains over 97% of the spatial variance in each velocity component. The fact that MAE and RMSE are nearly coincident further implies a negligible incidence of large outlier errors. Taken together, these metrics confirm that the model yields highly reliable reconstructions of the U and V fields.

In contrast, the sparse test-set performance collapsed: the model explained almost no variance (e.g. $R^2_U \approx 0.0086$, $R^2_V \approx -98.3727$) and produced $RMSE_U \approx 0.0920$ and $RMSE_V \approx 0.8686$, nearly an order of magnitude larger than in the dense case. This failure arises from both large gaps in the input fields and the resulting inaccurate velocity estimates.

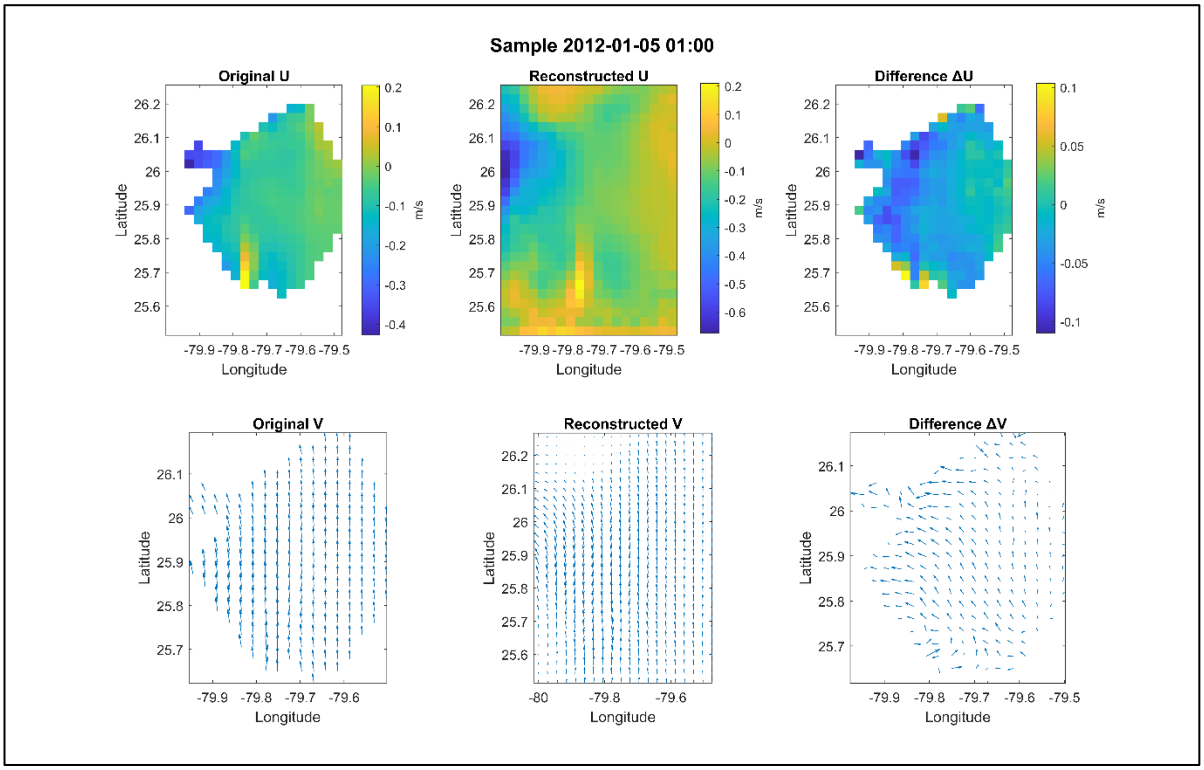

Figure 1: Reconstruction of ocean current fields for 2012-01-05 01:00 UTC in the standard test set

3. Current Boundary Detection via Attention U-net

SST and SSCa datasets used in this work are the same as in [1] and are processed in the same manner prior to the data fusion model pre-processing steps. The attention U-Net follows the same four-stage Conv–BN–ReLU encoder and symmetric upsampling decoder as a standard U-Net, but before each skip-connection it applies an attention block that computes a sigmoid mask from the decoder's gating signal and encoder features—filtering and weighting the encoder maps to focus on the most relevant spatial regions—then concatenates, conv-blocks them, and finishes with a 1×1 sigmoid output.

3.1. Data Pre-processing and Labeling

Each raw field (SST and SSCa) was first normalized independently to the range of 0–1. Once normalized, the SST field was downsampled to the native spatial resolution of the SSCa grid using bilinear interpolation. The co-registered fields were then stacked along the "channel" axis, yielding an input tensor of shape (H, W, C). For example, with two channels—normalized SST and normalized SSCa—the tensor has shape (H, W, 2), ready for patch extraction.

To generate boundary labels, a Sobel filter was applied independently to each of two channels (e.g., SST and SSCa), producing gradient magnitude maps that highlight sharp thermal or biological fronts. These two Sobel outputs were then combined via a pixel-wise maximum to capture features present in either field. A small Gaussian blur was applied to suppress noise, and the resulting smoothed map was thresholded to yield a binary edge mask. Finally, morphological skeletonization reduced these wide regions of high gradient to one-pixel-wide centerlines, creating crisp, topologically consistent boundary labels for supervision. An example of one of these labels can be seen in the bottom right of Figure 2, where the final pre-processed ground truth boundary map is shown.

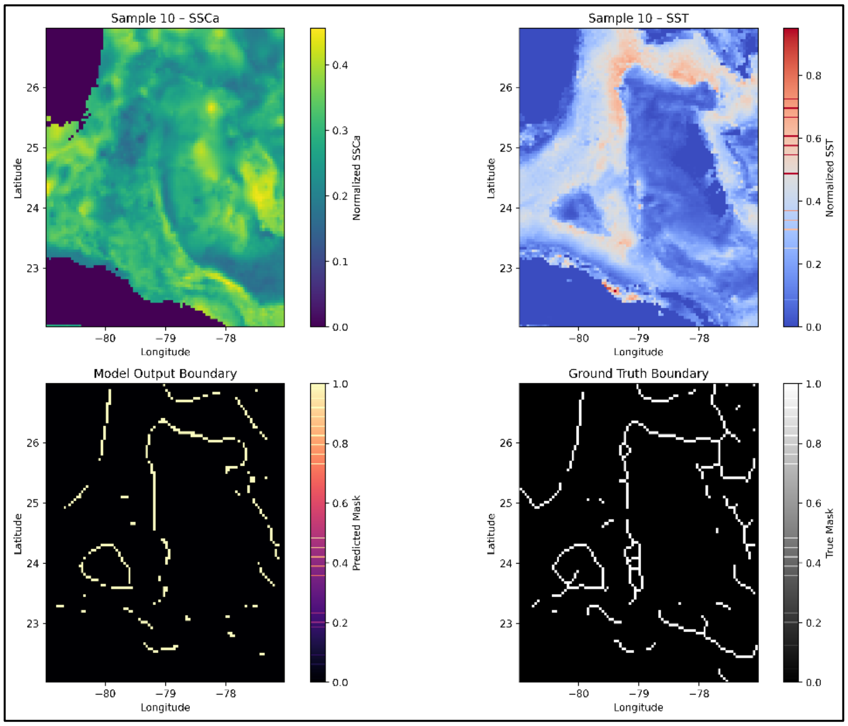

Figure 2: Attention U-net model result sample

3.2. Attention U-net Edge Detection Results

The top of Figure 2 shows the two input channels: normalized SSCa data on the left and normalized SST data on the right. The bottom of Figure 2 shows the model output on the right and the ground truth based on the pre-processed labels. The attention U-Net achieved a test loss of 0.0871 and an accuracy of 97.17%, yet only an Intersection-over-Union (IoU) of 0.2208, indicating that it identifies background pixels very well but struggles to localize sparse, one-pixel edges. By suppressing low-amplitude, noise-driven gradients in the ground truth, the model implicitly denoises the labels and produces cleaner boundaries—at the cost of the IoU, which penalizes all missed pixels equally. Lowering the Sobel threshold or adding noise-aware loss weighting could help capture those fainter features.

4. Conclusion

Dense reconstructions of the zonal (east–west) and meridional (north–south) velocity fields achieved an RMSE of less than 0.05 m/s and an R^2 greater than 0.97, demonstrating very high-fidelity recovery when data are plentiful. In contrast, reconstructions on the sparse test set saw RMSE values up to 0.09 m/s and virtually zero explained variance—highlighting the need to incorporate temporal-sequence models (for example, recurrent architectures) to exploit information across time and improve results when spatial coverage is limited.

Boundary detection was carried out using Sobel-gradient extraction followed by customized thresholding, morphological cleaning and denoising—instead of a one-step Canny filter—to retain fine control over each preprocessing stage and enhance label quality. This approach yielded an accuracy of 97.17 %.

Future work will refine these methods to map and predict the western boundary of the Gulf Stream, sub-mesoscale eddies, and future flow patterns. Comparative studies will be carried out to demonstrate the superiority of the proposed methodology.

5. Acknowledgements

This work was supported by the U.S. Department of Energy (DOE) under grant number DE-EE0011382. This work was also supported by the Florida Power & Light (FPL) Center of Intelligent Energy Technologies (InETech).

References

[1] Louis DeVito, James VanZwieten, and Yufei Tang. Comparative Evaluation of Ocean Current Flow Feature Detection Success based on Data Type within the Florida Straits. 2024.

[2] Marina DaSilva, Louis DeVito, James VanZwieten, and Yufei Tang. Evaluation of Flow Features Responsible for Extreme Events at a Potential Ocean Current Energy Extraction Location within the Gulf Stream. 2024.

[3] Nathachai Thongniran, et. al. Spatio-Temporal Deep Learning for Ocean Current Prediction Based on HF Radar Data. In 16th International Joint Conference on Computer Science and Software Engineering (JCSSE), pages 254–259, July 2019.

[4] Arnon Jirakittayakorn, Teeranai Kormongkolkul, Peerapon Vateekul, Kulsawasd Jitkajornwanich,and Siam Lawawirojwong. Temporal kNN for short-term ocean current prediction based on HF radar observations. In 2017 14th International Joint Conference on Computer Science and Software Engineering (JCSSE), pages 1–6, NakhonSiThammarat, Thailand, July 2017. IEEE.

[5] Ali Muhamed Ali, Hanqi Zhuang, Yu Huang, Ali K. Ibrahim, Ali Salem Altaher, and Laurent M. Chérubin. Ocean Currents Velocity Hindcast and Forecast Bias Correction Using a Deep-Learning Approach. Journal of Marine Science and Engineering, 12(9):1680, September 2024.

[6] Alisa Kugusheva, Hannah Bull, Evangelos Moschos, Artemis Ioannou, Briac Le Vu, and Alexandre Stegner. Ocean Satellite Data Fusion for High-Resolution Surface Current Maps. Remote Sensing, 16(7):1182, January 2024. Number: 7 Publisher: Multidisciplinary Digital Publishing Institute.

[7] Alexandre Immas, Ninh Do, and Mohammad-Reza Alam. Real-time in situ prediction of ocean currents. Ocean Engineering, 228:108922, May 2021.

[8] Anirban Sinha and Ryan Abernathey. Estimating Ocean Surface Currents with Machine Learning. Frontiers in Marine Science, 8:672477, June 2021.

[9] Lu Zhang, Wenyang Duan, Xinmiao Cui, Yuliang Liu, and Limin Huang. Surface current prediction based on a physics-informed deep learning model. Applied Ocean Research, 148:104005, July 2024.

[10] Simone Cosoli and Badema Grcic. IMOS - Ocean Radar - Quality Control procedures for IMOS Ocean Radar Manual. Technical report, Australian Ocean Data Network, 2019.

[11] Rick Chapman and Hans Graber. Validation of HF Radar Measurements. Oceanography, 10(2), 1997. Publisher: The Oceanography Society.